Journal of Power Sources 187 (2009) 74–79

Contents lists available at ScienceDirect

Journal of Power Sources

journal homepage: www.elsevier.com/locate/jpowsour

Short communication

Interlayer-free nanostructured $La_{0.58}Sr_{0.4}Co_{0.2}Fe_{0.8}O_{3-\delta}$ cathode on scandium stabilized zirconia electrolyte for intermediate-temperature solid oxide fuel cells

Seungho Lee [a], Hwa Seob Song [a], Sang Hoon Hyun [a], Joosun Kim [b], Jooho Moon [a,*]

[a] Department of Materials Science and Engineering, Yonsei University, 134 Shinchon-dong, Seodaemun-gu, Seoul 120-749, Republic of Korea
[b] Center for Energy Materials Research, Korea Institute of Science and Technology, Seoul 136-791, Republic of Korea

ARTICLE INFO

Article history:
Received 10 July 2008
Received in revised form 28 August 2008
Accepted 15 October 2008
Available online 5 November 2008

Keywords:
Solid oxide fuel cell
Cathode
LSCF
Interlayer-free electrode
Mixed ionic electronic conductor

ABSTRACT

LSCF powders with a specific surface area of 25.2 $m^2\,g^{-1}$ and an average particle size of 89 nm are synthesized by the polymerizable complex method. The use of nanocrystalline LSCF powders allows the fabrication of an interlayer-free nanoporous cathode on top of an ScSZ electrolyte at a low temperature at which non-electrocatalytic secondary phases cannot form. The electrochemical performance of the interlayer-free cathode depends largely on the sintering temperature. A cathode sintered at below 750 °C lacks sufficient mechanical adhesion to the electrolyte, while the electrode surfaces are locally densified when sintered at above 800 °C. Impedance spectroscopy combined with microstructural evidence reveals that the optimum sintering temperature for LSCF is 750 °C. This avoids excess densification and grain growth, and results in the lowest polarization resistance (0.048 $\Omega\,cm^2$ at 750 °C).

1. Introduction

Solid oxide fuel cells (SOFCs) are promising electrical power generators due to their high-energy conversion efficiency, low pollution emissions, and highly flexible operation with various fuels. Recently, significant effort has been devoted to the development of intermediate-temperature (600–800 °C) SOFCs (IT-SOFCs) because they facilitate the use of cheaper component materials and possibly offer long-term stability [1,2]. A $La_{1-x}Sr_xMn_yO_{3-\delta}$ (LSM)–YSZ composite has been frequently employed as a high-temperature cathode material because of its high electrochemical activity for the oxygen reduction reaction and good stability and compatibility with yttria-stabilized zirconia (YSZ) electrolyte. However, it is inapplicable for IT-SOFCs due to its deteriorated oxygen ion conductivity and high activation energy at 600–800 °C. As alternatives, mixed ionic electronic conductors (MIECs) such as $La_{0.6}Sr_{0.4}Co_{0.2}Fe_{0.8}O_3$, $Sm_{0.5}Sr_{0.5}CoO_3$, and $Ba_{0.5}Sr_{0.5}Co_{0.2}Fe_{0.8}O_3$ have been extensively investigated. Among these materials, $La_xSr_{1-x}Co_yFe_{1-y}O_{3-\delta}$ (LSCF) possesses a thermal expansion coefficient (TEC) that is well-matched with the zirconia-based electrolyte material, a high conductivity and good catalytic activity for the cathodic reaction [3–5].

In general, LSCF cathode fabrication involves heat-treatment at temperatures above 900 °C in order to obtain sufficient connectivities between cathode particles and cathode-electrolytes. Solid-state reactions may, however, occur between the LSCF cathode and zirconia-based electrolytes at above this temperature and form insulating zirconate phases such as $SrZrO_3$. In this regard, $Ce_{0.8}Gd_{0.2}O_{2-\delta}$ (CGO) is commonly inserted as a buffer layer in order to avoid undesired reactions [6]. The introduction of an interlayer may produce complexity in the cell structure, increases in the manufacturing cost and time, and instability due to the TEC mismatch between CGO and scandia-stabilized zirconia (ScSZ). In this regard, it was recently reported [7,8] that LSCF powders prepared by the citrate method can be utilized to form the cathode directly on the ScSZ electrolyte without interlayers by sintering below 900 °C.

For fabrication of interlayer-free LSCF-based cathodes, starting powders should be reactive at a temperature below 900 °C. LSCF powder characteristics and processing conditions determine the resulting cathode microstructure, which in turn strongly influences cell performance. Using nanoparticle-based cathode materials may allow us to enlarge the catalytic reaction site. In particular, entire electrode surfaces of MIECs can serve as an oxygen catalytic reaction, i.e., triple phase boundary (TPB), unlike with LSM/YSZ composite. Therefore, the use of nanoparticles not only allows for a ceria interlayer-free LSCF cathode, but it also results in enhanced electrochemical reaction sites, which improve cell performance. Nevertheless, using smaller powders does not always guarantee

* Corresponding author. Tel.: +82 2 2123 2855; fax: +82 2 365 5882.
E-mail address: jmoon@yonsei.ac.kr (J. Moon).

0378-7753/$ – see front matter © 2008 Elsevier B.V. All rights reserved.
doi:10.1016/j.jpowsour.2008.10.101

a higher cathodic performance since they might undergo excess densification and coarsening at high temperatures. Thus, optimum sintering conditions with respect to the starting particles is the key to balancing between the two conflicting factors, namely, porosity and particle connectivity. In this work, the influence of LSCF starting nanoparticle characteristics on cathodic polarization is investigated as a function of the sintering temperature. This is of considerable practical importance.

2. Experimental

The LSCF cathode powders were prepared by the Pechini-type polymerizable complex method [9,10]. Nitrate salts of La, Sr, Co, and Fe were dissolved in water at a molar ratio of 2.9:2:1:4 ($La_{0.58}Sr_{0.4}Co_{0.2}$ $Fe_{0.8}O_{3-\delta}$). Then, ethylene glycol and citric acid were added to bind the metal cations. After a polymerization reaction at 100 °C, the polymer gel was charred at 400 °C to remove organics and nitrates. To synthesize crystalline LSCF particles with varying particle sizes, the charred gel was calcined for 4 h at temperatures that ranged between 700 °C (denoted LSCF700) and 1000 °C (denoted LSCF1000). The particle size was determined with a laser scattering particle size analyzer (Nanotrac 150, Microtrac Inc., Montgomeryville, PA, USA). The Brunauer–Emmett–Teller (BET, Micromeritics ASAP2010) gas adsorption technique, X-ray diffraction (XRD, Rigaku D/max-Rint2100) and field emission scanning electron microscopy (FE-SEM, FEG XL 30, FEI) were used to characterize the synthesized LSCF powders. The densification behaviour of the LSCF powders prepared by different calcination temperatures was analyzed with a dilatometer (DIL402C, NETZSCH).

An electrolyte-supported symmetric LSCF/ScSZ/LSCF cell was fabricated. First, commercially available ScSZ powders (89 mol% ZrO_2–10 mol% Sc_2O_3–1 mol% Al_2O_3, AGC Seimi Chemical Co. Ltd., Japan) were pressed into a pellet and sintered at 1400 °C for 4 h in air. An ScSZ disk with a diameter of 25 mm and a thickness of 0.5 mm was obtained. An LSCF cathode layer was deposited on both sides of the SCSZ electrolyte by screen-printing using paste materials that were a mixture of the powders and additives dispersed in an organic solvent, followed by firing for 2 h at temperatures between 700 and 1000 °C. After sintering, a platinum mesh connected to a platinum wire was attached to the cathode layer for current-collection by means of platinum paste. The area of the applied cathode was 1.4 cm^2 and the thickness was about 10 μm.

The cell microstructure was investigated by means of FE-SEM. XRD was used to determine whether chemical reactions occur when the LSCF800-ScSZ composite (1:1 in a weight ratio) is subjected to firing at varying temperatures (800–1100 °C). An electron probe micro-analyzer (EPMA, EPMA1600, SHIMADZU) was also employed to analyze chemical reactions at the interface between LSCF and ScSZ, when sintered in the temperature range of 700–900 °C. Electrochemical impedance measurements were performed on the symmetrical cells at various partial oxygen pressures using a Solatron SI 1260/1287 instrument. Impedance spectra were obtained over a frequency range from 100 kHz to 0.1 Hz with an ac voltage of 20 mV at temperatures ranging from 600 to 750 °C in 50 °C intervals.

3. Results and discussion

Well-distributed nano-sized LSCF powders were synthesized by the Pechini-type polymerizable complex technique. Laser scattering investigations reveal that the calcination temperature influences the particle size of the LSCF powders. The average sizes of LSCF700 and LSCF1000 were determined to be 88.7 and 385 nm, respectively, as shown in Table 1. The method produced much smaller LSCF powders than other synthesis routes, even when calcined at the same temperature. For instance, the mean size of LSCF powder prepared by a citrate method at 1000 °C was reported to be 550–660 nm [8]. The surface area of the LSCF powders was also significantly influenced by the calcination temperature; it ranged from 25.2 $m^2\,g^{-1}$ at 700 °C to 1.73 $m^2\,g^{-1}$ at 1000 °C (see Table 1). The different particle characteristics of the LSCF powders will also influence the optimum firing temperature and the resulting sintered microstructure of the cathode.

Table 1
Surface area and particle size of synthesized LCSF powder as function of calcination temperature.

Powder type	LSCF700	LSCF800	LSCF900	LSCF1000
Surface area ($m^2\,g^{-1}$)	25.2	13.6	5.08	1.73
Particle size (D50) (nm)	88.7	127.0	264.7	385.0

Besides the physical characteristics, the phase purity and the crystallinity of the particles are also important factors for perovskite cathode materials. Fig. 1a shows XRD patterns as a function of the calcination temperature. All the synthesized LSCF powders that were calcined above 700 °C exhibit a crystalline phase with a rhombohedral perovskite structure and no impurity phase, while other synthesis methods require at least 800 °C to prepare phase-pure LSCF [11]. The chemical stability between the LSCF and ScSZ was also investigated by XRD analysis in order to determine the maximum sintering temperature for the formation of an interlayer-free LSCF cathode on ScSZ electrolytes. Apart from LSCF and ScSZ, there are no other phases in the samples sintered below 800 °C. By con-

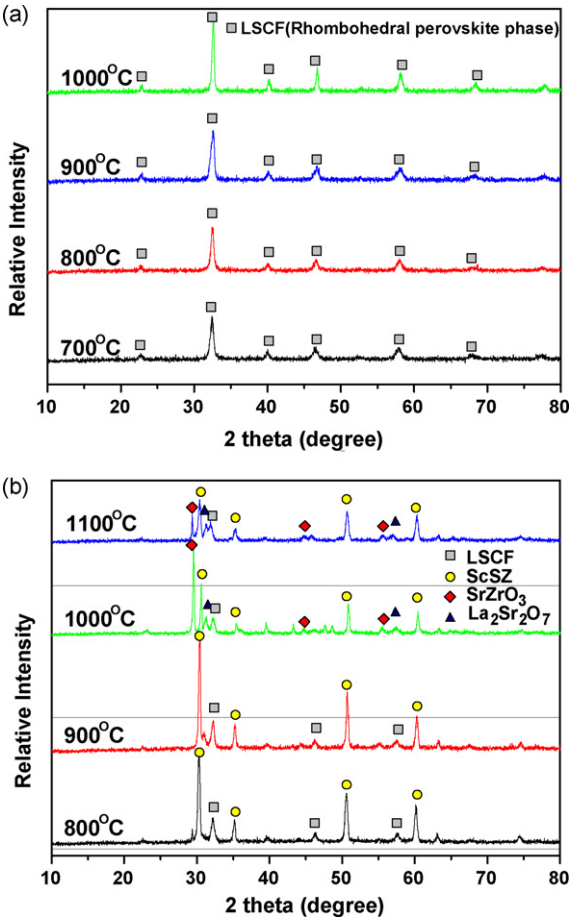

Fig. 1. X-ray diffraction patterns: (a) crystallization behaviour of Pechini method-derived LSCF powders as function of calcination temperature; (b) mixture of LSCF and ScSZ powders fired at varying temperatures.

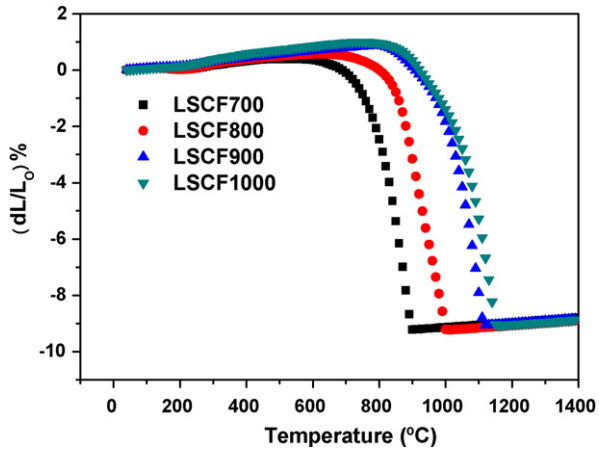

Fig. 2. Shrinkage behaviour of LSCF base samples as function of sintering temperature.

trast, secondary phases such as $SrZrO_3$ and $La_2Zr_2O_7$ are observed in samples sintered above 1000 °C. This implies that an interlayer between the LSCF cathode and ScSZ electrolyte is necessary to prevent the formation of non-electrocatalytic secondary phases. It also indicates that firing below 900 °C may enable the fabrication of an interlayer-free LSCF cathode/ScSZ electrode structure as long as the LSCF undergoes sufficient densification at such a low temperature.

The densification behaviour of LSCF powders prepared by different calcination temperatures is illustrated in Fig. 2. The shrinkage onset temperature varies depending on the physical characteristics of the LSCF. Shrinkage of a bar sample made with the smallest size (LSCF700) starts at ~550 °C but ceases at ~900 °C, whereas LSCF800 undergoes densification at ~630 °C that is completed at ~1000 °C. Samples with larger sizes (LSCF900 and LSCF1000) begin to shrink at ~810 °C. These findings mean that a nano-sized powder calcined at a lower temperature has a higher sintering activity than a larger powder. Due to the similar initial packing densities of the bar samples made of these powders, the linear shrinkages are all nearly 9.21%. The dilatometer results clearly show that fabrication of a cathode using both LSCF700 and LSCF800 powders is possible.

Polarization resistances for cathodes made of either LSCF700 or LSCF800 are presented in Fig. 3a. The area specific resistance (ASR) of the electrode polarization is lower for the cathode prepared with a smaller particle size (LSCF700) over the entire temperature range (600–750 °C). The area specific resistance is 0.125 Ω cm^2 at 700 °C for LSCF700 and 0.18 Ω cm^2 for LSCF800. The surface area of the LSCF700 starting powders is approximately twise that of the LSCF800. A difference in the ASR is more noticeable in the low temperature range (600–650 °C), possibly indicating that a nano-sized starting powder would be beneficial for the fabrication of IT-SOFC cathodes.

Nanopowders with a large surface area may prove unstable at elevated temperatures. The usual operational temperature for IT-SOFCs is too close to the calcination and processing temperatures of the LSCF700 cathode sintered at 700 °C. While the initial cathodic performance may be superior, it is likely that there will be poor long-term stability due to significant grain growth of nanopowders and densification of the porous electrode [12,13]. Furthermore, the adhesion strength between the electrode and the electrolyte will not be sufficiently strong to withstand thermocyclic stress during operation. We actually found that the LSCF700 cathode layer has become partially detached after testing. As a result, the LSCF700 powders were excluded from further studies.

The sintering temperature affects the microstructure of the electrode, its adhesion to the electrolyte, and the reactivity between the

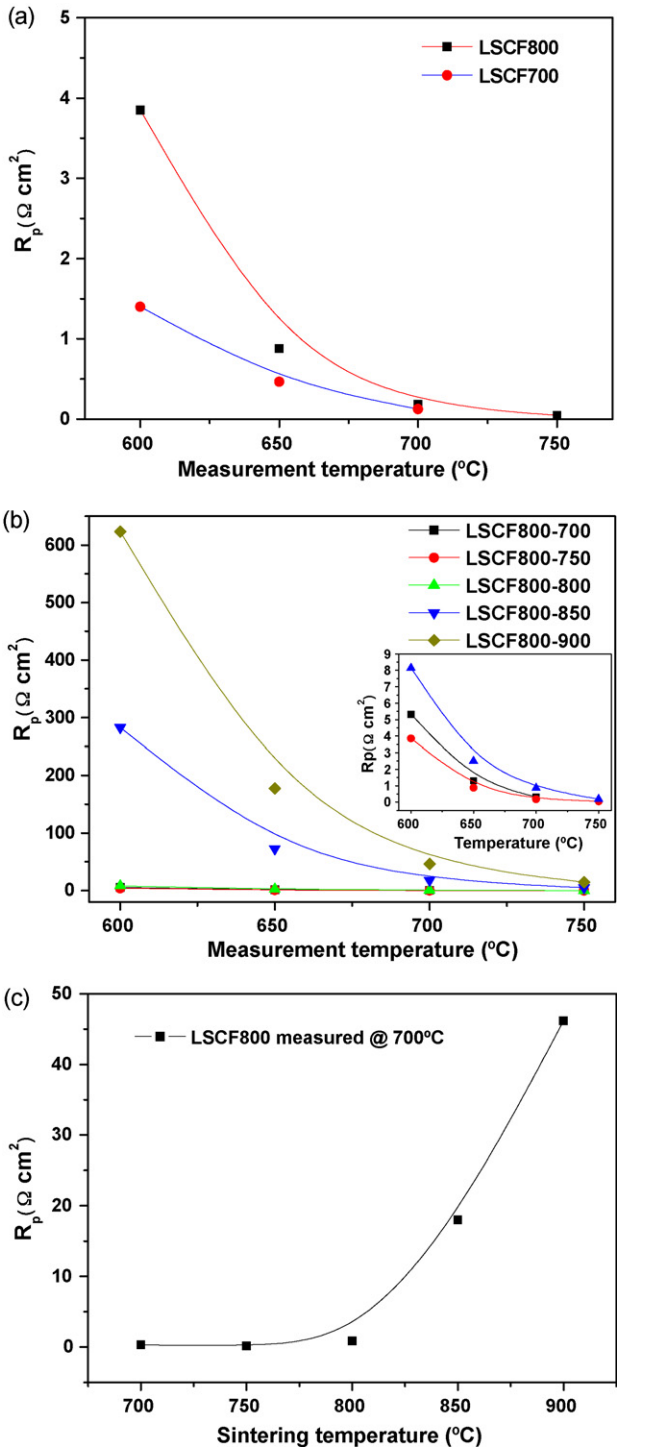

Fig. 3. Polarization resistance (R_p) of interlayer-free LSCF cathodes: (a) as function of calcination temperature; (b) LSCF800 cathode measured over temperature range of 600–750 °C; (c) LSCF800 cathode measured at 750 °C as function of sintering temperature.

LSCF cathode and ScSZ electrolyte. The cathode performance of a symmetric cell LSCF800/ScSZ/LSCF800 as a function of sintering temperature is shown in Fig. 3b. The cell with a cathode sintered at 750 °C gives the best performance, i.e., ~0.048 Ω cm^2 at 750 °C. To the best of our knowledge, this is the lowest ASR associated with an LSCF cathode yet to be reported [14]. The ionic conductivity and catalytic activity of a single-phase LSCF cathode decrease

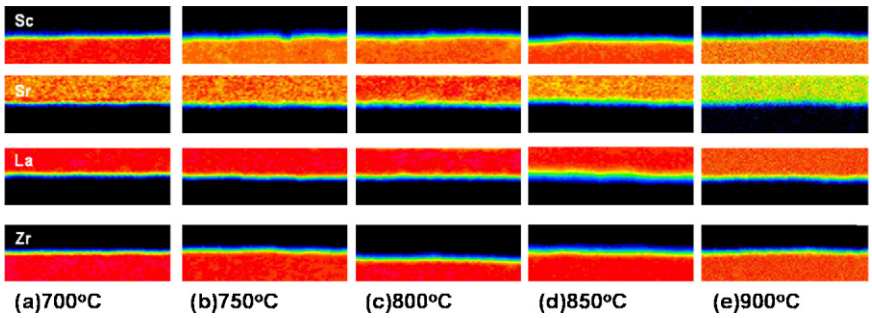

Fig. 4. EPMA compositional mapping data for Sc, Sr, La and Zr elements obtained from cross-section of LSCF|ScSZ interface fired at different temperatures: (a) 700 °C, (b) 750 °C, (c) 800 °C, (d) 850 °C and (e) 900 °C. Scanned area is 18.1 μm in width and 5 μm in height.

exponentially with decreasing temperature, so that the polarization resistance sharply increases as the temperature goes down. It has been reported that the polarization resistance can be reduced further by utilizing either a LSCF-SDC or LSCF-GDC composite cathode [15,16].

The polarization resistance of a LSCF800 cathode on a ScSZ electrolyte measured at 700 °C is given in Fig. 3c as a function of sintering temperature. The resistance remains low at temperatures between 700 and 800 °C and then increases rapidly above 800 °C. The minimum ASR (~0.18 Ω cm^2) is observed when the sintering temperature is 750 °C. Cathodic performance degradation above 800 °C can be attributed either to physical variation (i.e., reduced reaction sites induced by grain growth and/or densification) or to chemical changes (i.e., formation of non-electrocatalytic

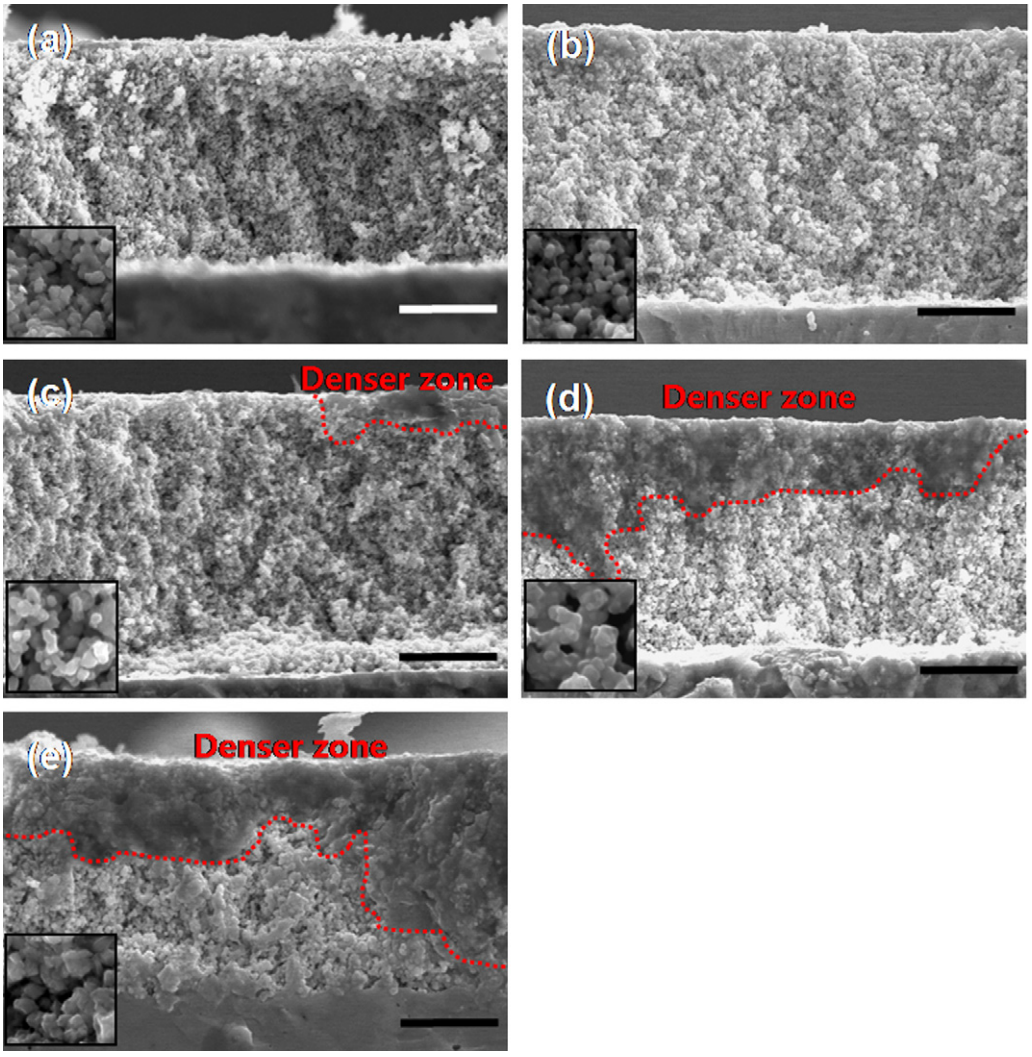

Fig. 5. SEM images of LSCF800 cathode at different temperatures: (a) 700 °C, (b) 750 °C, (c) 800 °C, (d) 850 °C, and (e) 900 °C. Scale bars represent 5 μm.

secondary phases at the interface). Although the secondary phase is not detected by XRD when sintered below 900 °C, we tried to determine the spatial distributions of La, Sr, Sc, and Zr elements across the LSCF|ScSZ interface by EMPA compositional mapping. As shown in Fig. 4, the LSCF|ScSZ maintains a clear compositional boundary and none of the metal cations diffuses across the interface to form electrochemically inactive La- or Sr-zirconia phases. This result clearly excludes the possibility of a chemical change explaining the cathodic performance degradation that occurs with sintering above 800 °C.

The cross-sectional microstructures of the LSCF electrode on the ScSZ electrolyte as a function of sintering temperature are presented in Fig. 5. The cathode microstructure is significantly influenced by the sintering temperature. Uniform nanoporous electrode structures firmly adher to the electrolyte when sintered at a temperature between 700 and 800 °C. By contrast, an electrode sintered at 850 °C experiences local densification, as illustrated by Fig. 5d. In particular, the surface region of the electrode is significantly densified without the constraint of an underlying dense electrolyte (Fig. 5e). This surface dense layer can limit the electrochemical reaction sites and prevent oxygen from diffusing through the electrode. Microstructural observations clearly reveal that the variation in the polarization resistance as a function of sintering temperature is due to physical changes in the electrode microstructure.

For quantitative analysis, impedance spectroscopy was utilized to analyze LSCF cathode performance. It has been reported [17,18] that the impedance spectrum of a composite cathode can be divided into two different arcs, denoted *resistance* A (R_A at high frequency) and *resistance* B (R_B at low frequency), each of which represents a dominant electrode kinetic process [17,18]. *Resistance* A can be influenced by the transport of oxygen ions through the LSCF. In other words, the magnitude of R_A relates to the phase interconnectivity between the LSCF powders. *Resistance* B, characterized by a strong oxygen pressure dependence, is presumably associated with the charge-transfer process that occurs at the reaction site. Thus, R_B mainly reflects electrochemical oxygen reduction on the cathode, which is a strong function of the reaction site density. Impedance analysis as a function of oxygen partial pressure provides a better understanding of the electrode polarization mechanism with respect to its microstructure variation.

The impedance spectra of LSCF cathode measured at 700 °C at both 0.21 and 1.0 atm P_{O_2} are illustrated in Fig. 6a. Impedance spectra for the MIECs could not be clearly divided into two primary arcs. The use of a different plot in which the difference in the derivative of the spectrum with respect to the frequency (f) obtained between a specific and reference oxygen partial pressure (i.e., $\Delta(\partial Z_{real}/\partial \log f) = (\partial Z^{\#\,atm\,P_{O_2}}_{real}/\partial \log f) - (\partial Z^{1\,atm\,P_{O_2}}_{real}/\partial \log f)$ is plotted against $\log f$ has been suggested [19,20]. Such a graphical representation allows determination of the frequency at which the resistance variation is most marked as a function of the oxygen partial pressure, as shown in Fig. 6b. The relative difference in the derivative of the resistance changes from a positive deviation to a negative deviation at $f = 79.4$ Hz. It reaches a maximum value at a nearly constant frequency of 25.1 Hz, regardless of P_{O_2}, which is characterized by a summit frequency (f^{SUM}) for the *resistance B* arc at a low-frequency region. The summit frequency for the *resistance* A arc in the high-frequency region is 630.7 Hz, as determined using an equivalent circuit model. The fitted spectrum is composed of two separated arcs located at the low and high summit frequencies and is well-matched with the experimentally obtained spectrum of the LCSF cathode (the red line in Fig. 6a). Thus, the sintering temperature induced variations of the electrode polarization can be understood via impedance analysis.

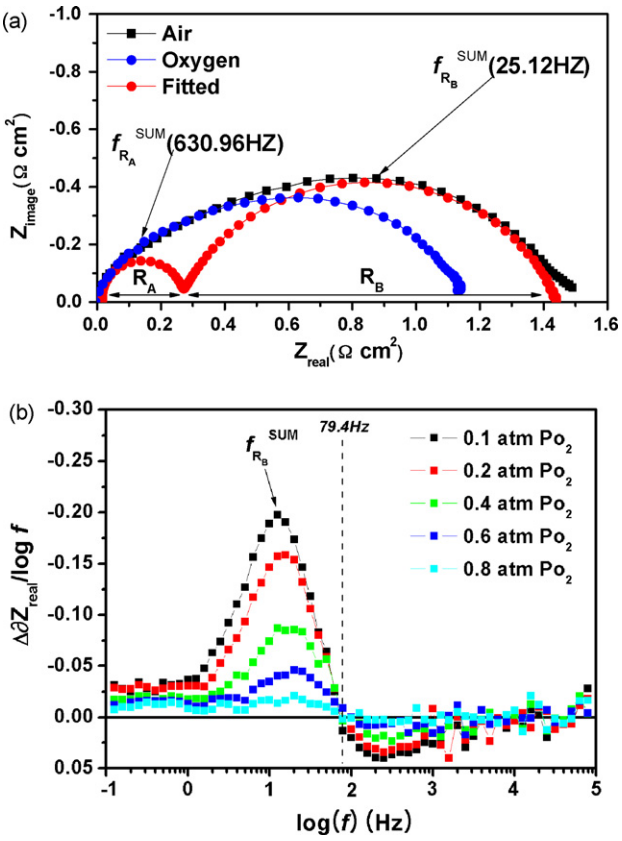

Fig. 6. (a) Nyquist plot of impedance of LSCF800 cathode sintered at 800 °C measured at 700 °C in air (squares) and in oxygen (circles), and deconvoluted arcs. (b) Difference plot of $\Delta(\partial Z_{real}/\partial \log f) = (\partial Z^{\#\,atm\,P_{O_2}}_{real}/\partial \log f) - (\partial Z^{1\,atm\,P_{O_2}}_{real}/\partial \log f)$ against log(f).

The interfacial polarization resistances separated into the R_A and R_B processes for symmetrical cells are given in Fig. 7 as a function of the sintering temperature. The R_A values are nearly independent of the sintering temperature, except for sintering at 900 °C. On the other hand, the R_B values sharply increase as the sintering temperature is raised from 800 to 900 °C. This indicates that the cathode degradation mechanism as a function of the sintering temperature is due to decreases in the electrocatalytic site (TPB) density associated with the cathode, which is strongly influenced by phys-

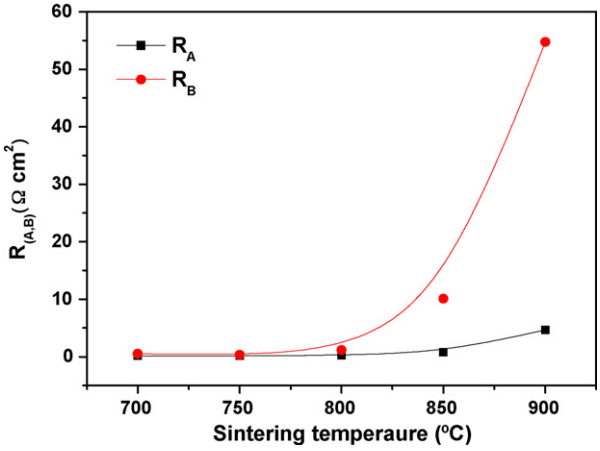

Fig. 7. Polarization resistance of process A (R_A) and process B (R_B) as a function of sintering temperature. Impedance spectra obtained in air using symmetrical cells and deconvoluted into two arcs using $f^{SUM}_{R_A}$ and $f^{SUM}_{R_B}$ determined in Fig. 6a.

ical microstructure variation, as shown in Fig. 5. Nanosized LSCF powders need to be sintered at the optimum temperature (750 °C). Otherwise, over-densification and excess grain growth lead to a loss of catalytic activity of the electrode as a result of the reduced surface reaction sites.

4. Conclusions

An interlayer-free LSCF cathode on top of an ScSZ electrolyte has been fabricated. The use of nanocrystalline LSCF powders enables the fabrication of a high-performance cathode with lower interfacial resistance and without the introduction of a GDC or SDC interlayer. The polarization resistance of the LSCF cathode is 0.048 $\Omega\,cm^2$ at 750 °C, which is the lowest value so far reported in the literature. Nanoporous cathodes that adher to the electrolyte are obtained from Pechini method-derived highly active LSCF nanopowders at temperatures low enough to prevent the formation of a non-electrocatalytic secondary phase at the LSCF|ScSZ interface. The electrochemical performance of the interlayer-free cathode depends largely on the sintering temperature. An optimum sintering temperature of 750 °C is chosen in order to avoid excess densification and grain growth, which adversely affect cathode performance. Impedance analysis, in conjunction with microstructural and compositional mapping analyses, reveal that the dependence of the interlayer-free LCSF cathode on the sintering temperature corresponds mainly to variation of the electrochemical reaction sites upon sintering.

Acknowledgements

The work was the outcome of a fostering project of the Specialized Graduate School of Hydrogen and Fuel Cell supported financially by the Ministry of Commerce, Industry and Energy (MOCIE) and Seoul R&BD Program (CS070157). It was also partially supported by the Korea Science and Engineering Foundation (KOSEF) through the National Research Laboratory Program funded by the Ministry of Science and Technology (No. R0A-2005-000-10011-0).

References

[1] B.C.H. Steele, A. Heinzel, Nature 414 (2001) 345–352.
[2] B.C.H. Steele, Solid State Ionics 134 (2000) 3–20.
[3] J.M. Serra, H.P. Buchkremer, J. Power Sources 172 (2007) 768–774.
[4] L.W. Tai, M.M. Nasrallah, H.U. Anderson, D.M. Sparlin, S.R. Sehlin, Solid State Ionics 76 (1995) 259–271.
[5] L.W. Tai, M.M. Nasrallah, H.U. Anderson, D.M. Sparlin, S.R. Sehlin, Solid State Ionics 76 (1995) 273–283.
[6] W.H. Kim, H.S. Song, J. Moon, H.W. Lee, Solid State Ionics 177 (2006) 3211–3216.
[7] Z. Lei, Q. Zhu, L. Zhao, J. Power Sources 161 (2006) 1169–1175.
[8] K. Murata, T. Fukui, H. Abe, M. Naito, K. Nogi, J. Power Sources 145 (2005) 257.
[9] M. Popa, J. Frantti, M. Kakihana, Solid State Ionics 154–155 (2002) 437–445.
[10] M. Kakihana, M. Arima, M. Yoshimura, N. Ikeda, Y. Sugitani, J. Alloys Compd. 283 (1999) 102–105.
[11] W. Jin, S. Li, P. Huang, N. Xu, J. Shi, J. Membr. Sci. 170 (2000) 9–17.
[12] J.H. Choi, J.H. Jang, J.H. Ryu, S.M. Oh, J. Power Sources 87 (2000) 92.
[13] M.J. Jorgensen, S. Primdahl, C. Bagger, M. Mogensen, Solid State Ionics 139 (2001) 1.
[14] F. Qiang, K. Sun, N. Zhang, X. Zhu, S. Le, D. Zhou, J. Power Sources 168 (2007) 338–345.
[15] E. Perry Murray, M.J. Sever, S.A. Barnett, Solid State Ionics 148 (2002) 27–34.
[16] C. Fu, K. Sun, N. Zhang, X. Chen, D. Zhou, Electrochim. Acta 52 (2007) 4589–4594.
[17] M.J. Jorgensen, M. Mogensen, J. Electrochem. Soc. 148 (2001) A433–A442.
[18] M. Juhl, S. Primdahl, M. Mogensen, in: F.W. Poulsen, N. Bonanos, S. Linderoth, M. Mogensen, B. Zachau-Christiansen (Eds.), High Temperature Electrochemistry: Ceramics and Metals, Risø National Laboratory, Denmark, 1996, pp. 295–301.
[19] R. Barfod, M. Mogensen, T. Klemensø, A. Hagen, Y. Liu, P.V. Hendriksen, J. Electrochem. Soc. 154 (4) (2007) B371–B378.
[20] S.H. Jensen, A. Hauch, P.V. Hendriksen, M. Mogensen, N. Bonanos, T. Jacobsen, J. Electrochem. Soc. 154 (12) (2007) B1325–B1330.